Inorganic Chemistry

Article

pubs.acs.org/IC

Surfactant-Free Synthesis, Luminescent Properties, and Drug-Release Properties of LaF_3 and $LaCO_3F$ Hollow Microspheres

Ruichan Lv, Shili Gai,* Yunlu Dai, Fei He, Na Niu, and Piaoping Yang*

Key Laboratory of Superlight Materials and Surface Technology, Ministry of Education, Harbin Engineering University, Harbin 150001, People's Republic of China

Supporting Information

ABSTRACT: Uniform LaF_3 and $LaCO_3F$ hollow microspheres were successfully synthesized through a surfactant-free route by employing $La(OH)CO_3$ colloidal microspheres as a sacrificial template and $NaBF_4$ as the fluorine source. The synthetic process consists of two steps: the preparation of a $La(OH)CO_3$ precursor via a facile urea-based precipitation and the following formation of lanthanide fluoride hollow microspheres under aqueous conditions at low temperature (50 °C) and short reaction time (3 h), without using any surfactant and catalyst. The formation of hollow spheres with controlled size can be assigned to the Kirkendall effect. It is found that the phase and structure of the products can be simply tuned by changing the pH values of the solution. Time-dependent experiments were employed to study the possible formation process. N_2 adsorption/desorption results indicate the mesoporous nature of LaF_3 hollow spheres. Yb^{3+}/Er^{3+} (Ho^{3+}) and Yb^{3+}/Tm^{3+}-doped LaF_3 hollow spheres exhibit characteristic up-conversion (UC) emissions of Er^{3+} (Ho^{3+}) and Tm^{3+} under 980 nm laser-diode excitation, and Ce^{3+}/Tb^{3+}-doped LaF_3 and $LaCO_3F$ emit bright yellow-green and near-white light under UV irradiation, respectively. In particular, LaF_3:Yb/Er and $LaCO_3F$:Ce/Tb hollow microspheres exhibit obvious sustained and pH-dependent doxorubicin release properties. The luminescent properties of the carriers allow them to be tracked or monitored during the release or therapy process, suggesting their high potential in the biomedical field.

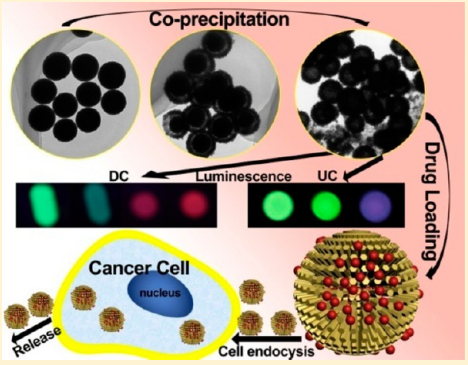

INTRODUCTION

In recent years, hollow-structured mesoporous spheres with photoluminescence (PL) properties aroused much attention because they have been extensively used as the most promising functional material in various biological fields such as drug carrying,[1,2] gene delivery,[3,4] cell labeling,[5,6] and photodynamic therapy.[7,8] In the fields of drug storage and delivery, hollow-structured materials have gained special attention because they simultaneously have large voids and mesoporous shells.[9−11] The large voids make it possible to store more drug molecules than conventional materials. Also, the mesoporous shells can provide accessible channels for drug molecule diffusion and mass transfer. On the other hand, they can control the permeability of the shells for matter exchange between the outer environment and voids. Currently, the synthesis and applications of rare-earth fluorides have attracted wide interest because they have very low vibrational energy and outstanding thermal and environmental stability, which result in minimization of the quenching concentration of the excited rare-earth ions and wide application as luminescent materials.[12−22] Among these rare-earth fluorides, the LaF_3 host matrix shows especially photochemical stability, excellent biocompatibility, and relatively lower crystalline temperature, and its phonon energy is as low as 350 cm^{-1}.[23] Therefore, LaF_3 was widely used as an up-conversion (UC) luminescent material,[24,25] and LaF_3 was also well accepted by doping with Eu^{3+} or special Ce^{3+}/Tb^{3+} ions, which possess strong red and green down-conversion (DC) luminescence, respectively.[26,27]

Because of the allegro preparation of rare-earth fluoride particles, many researches on the synthetic methods are focused on various structures with self-assembling nanocrystals, such as fullerene-like, bundlelike, rodlike, disklike, and spindlelike morphologies with different crystalline phases.[28−31] However, with the combinational development of nanotechnology and biomedicine, rare-earth fluoride nano/microparticles with functional structures have significant material-to-biological application in place of these simply luminescent matrixes. Meanwhile, in order to obtain a beautiful shape for uniform hollow spheres, the hard templates, such as silica,[32,33] carbon spheres,[34] MFs,[35,36] and polystyrene beads,[37,38] have usually been used as antecedent templates, and hollow spheres were prepared after depriving the templates. However, this method has the disadvantages of a complicated process and low yield, as well as strong acid/alkali/oxidant and calcinations used during the removal process, which raise environmental pollution and energy consumption. In order to remedy these drawbacks, sacrificed templates are reported to acquire hollow spheres via the Ostwald theory[39] and Kikendall effect.[40] Zhang et al.[41] have proposed one precursor (Y_2O_3) to prepare the $NaYF_4$ hollow

Received: September 30, 2013
Published: December 23, 2013

   dx.doi.org/10.1021/ic402468k | Inorg. Chem. 2014, 53, 998−1008

fluoride spheres. However, in his method, HF was used as the pH-regulating solution and assistant fluorine source, which can seriously damage human organs after indrafting or touching. Also, the precursor needed a calcination process, which was cumbersome and complicated. Meanwhile, the limited volume of the autoclave used in the hydrothermal process also leads to low yield.[42] Compared with hydrothermal,[43] electrospinning,[44] and other related synthetic processes, the coprecipitation synthesis has superior characteristics, such as simpler facilities, lower reaction cost, and higher yield without high temperature or pressure. In this regard, the coprecipitation route as a large-scale and facile approach to synthesizing functional mesoporous materials should have a high potential for research and actual applications. All in all, a surfactant-free, low-consumption, and mass-production method to prepare uniform hollow structures with multiple functions is still challenging to researchers. It is essential and significant to develop simple methods to prepare rare-earth fluoride particles with hollow mesoporous structure under mild reaction conditions.

In this report, we proposed a facile, mild, and mass-production method to synthesize pure mesoporous LaF_3 and $LaCO_3F$ hollow spheres by only adjusting the initial pH value. There are three advantages to our synthetic method. First, $La(OH)CO_3$ was prepared as the sacrificed template, and $NaBF_4$ was used as the fluorine source, which masterfully controlled the resulting morphology. Second, the facile and mass-production coprecipitating process proposed is carried out under very low temperature (50 °C) and short time (3 h). Third, the entire process was conducted in an aqueous solution without any surfactant or catalyst added. Meanwhile, the UC luminescent properties of LaF_3 doped with Yb^{3+}/Er^{3+}, Yb^{3+}/Ho^{+}, and Yb^{3+}/Tm^{3+} under 980 nm laser-diode (LD) irradiation and the DC luminescent properties of LaF_3 and $LaCO_3F$ doped with Ce^{3+}/Tb^{3+} and Eu^{3+} under UV irradiation were investigated in detail and emit strong and tunable light. Moreover, as a potential biomaterial, doxorubicin loading and release measurements were also carried out.

EXPERIMENTAL SECTION

Reagents and Materials. All of the chemical reagents used in this experiment are of analytical grade without any further purification, including urea, sodium fluoroborate ($NaBF_4$; Beijing Chemical Corp.), La_2O_3 (99.99%), Yb_2O_3 (99.99%), Er_2O_3, Ho_2O_3, Tm_2O_3, Ce_2O_3, Tb_4O_7, and Eu_2O_3 (99.99%; Sinopharm Chemical Reagent Co., Ltd.), phosphate-buffered saline (PBS), and potassium hydrogen phthalate (PHP; Tianjin Kermel Chemical Reagent Co., Ltd.).

Synthesis. *Synthesis of $La(OH)CO_3:Ln^{3+}$ Microspheres.* $La(OH)CO_3$ microspheres were prepared via a urea-based precipitation process according to a published report[45] with slight modification. In a typical process, 0.5 M $La(NO_3)_3$ were prepared by dissolving the corresponding calculated La_2O_3 into HNO_3 with gradual heating. A total of 1 mL of 0.5 M $La(NO_3)_3$ and 1.5 g of urea were dissolved in 50 mL of deionized water in a beaker. After stirring for 5 min, the mixture was kept heating at 90 °C for 2 h through a water bath. The resulting mixture was centrifuged at 6000 rpm for 4 min. The supernatant solution was discarded, and the precipitate was saved with fresh deionized water. After this process was repeated three times, $La(OH)CO_3$ was acquired. The preparation of $La(OH)CO_3:Ln^{3+}$ microspheres was similar to the procedure above with a calculated lanthanide value.

Synthesis of $LaF_3:Ln^{3+}$ and $LaCO_3F:Ln^{3+}$. The as-prepared 0.5 mmol $La(OH)CO_3$ sample was dissolved by 10 mL of deionized water, and then 0.44 g of $NaBF_4$ was added with continuous stirring. After the solution appeared to be uniform, the beaker was transferred to a water bath kettle at 50 °C. A diluted HNO_3 solution was used to regulate the pH value. After 3 h of reaction, the resulting product was centrifuged three times and dried in a baking oven for 12 h to obtain a LaF_3 sample. A $LaCO_3F$ sample was obtained by the same process but with the initial pH value unregulated.

In Vitro Viability of LaF_3:Yb/Er ($LaCO_3F$ Ce/Tb). In a typical procedure, a 5 mg/mL MTT solution was prepared by PBS. A total of 200 mL of material per well plated with 5000−6000 L929 fibroblast cells was put in a 96-well plate. For blank controls, eight wells were left empty and then incubated 24 h in order to make the cells attach to wells with 5% CO_2 at 37 °C. LaF_3:Yb/Er and $LaCO_3F$:Ce/Tb samples were sterilized via UV irradiation for 2 h. After that, they were diluted to the respective concentrations of 7.8125, 15.625, 31.25, and 62.5 μg/mL, and then the solutions were added to the wells and incubated for another 24 h at 37 °C with 5% CO_2. A total of 20 μL of the prepared MTT solution was added to each well with different amounts. The plate was subsequently incubated for another 4 h at 37 °C. Meanwhile, viable cells make MTT reduce to formazan, which can be dissolved by dimethyl sulfoxide. After that, 100 mL of acidified isopropyl alcohol was added to each well and placed on a shaking table for 5 min of 150 rpm in order to blend the formazan and solvent completely. The absorbance was recorded using a microplate reader regulated to 570 nm. The optical density, which received no polymer or drug, was regarded as 100% growth.

Doxorubicin (DOX) Loading and Release Test. A total of 0.03 g each of the LaF_3:Yb/Er and $LaCO_3F$:Ce/Tb samples were added to 5 mL of PBS and ultrasonically dispersed. After that, 0.0025 g of DOX was added to the solution with slow stirring at room temperature for 24 h. The as-prepared mixture was centrifugally separated at 6000 rpm for 4 min, and then the supernatant solution was kept for UV−vis analysis. A total of 10 mL of fresh PBS was replenished in the centrifugal tube and set in a water bath kettle at 37 °C with magnetic stirring for 10 min, and the supernatant solution was maintained. The process was repeated, and the release time was changed as 20 min, 30 min, 40 min, 50 min, 60 min, 2 h, 4 h, 6 h, 8 h, 12 h, 24 h, and 48 h, respectively. PBS (pH = 7) and PHP (pH = 4) were prepared directly by a pH modifier.

The loading amount and concentration of DOX in the solution were determined by UV−vis absorption measurement. Figure S1A in the Supporting Information (SI) shows the absorption spectrum of DOX between 350 and 600 nm, and the peak at 480 nm was used as the typical absorbance of the estimated solution. The relationship between the absorbance at 480 nm and the concentration of a standard DOX solution is given in Figure S1B in the SI. Through testing of the absorbance of the supernatant at 480 nm with different release times, the mass of DOX was acquired by conversion of the absorbance to concentration with the volume multiplied.

The loading amount (M_{LA}) can be calculated using the formula

$$M_{LA} = O_{DOX} - R_{DOX}$$

where O_{DOX} is the original DOX concentration and R_{DOX} is the residual concentration.

The loading efficiency (LE %) can be calculated using the formula

$$LE\ \% = M_{LA}/O_{DOX}$$

The release efficiency (RE %) can be calculated using the formula

$$RE\ \% = \sum M_{DOX\ in\ supernatant}/M_{LA}$$

where $M_{DOX\ in\ supernatant}$ is the DOX concentration in the supernatant with different release times.

Characterization. Powder X-ray diffraction (XRD) measurements were performed on a Rigaku D/max TTR-III diffractometer at a scanning rate of 15°/min in the 2θ range from 20° to 80°, with graphite-monochromatized Cu Kα radiation (λ = 0.15405 nm). Images were obtained digitally by scanning electron microscopy (SEM; JSM-6480A), transmission electron microscopy (TEM; FEI Tecnai G^2 S-Twin), and high-resolution TEM (HRTEM). N_2 adsorption/desorption isotherms were obtained on a Micromeritics ASAP 2010 apparatus. The pore-size distribution was calculated from the adsorption branch of a N_2 adsorption/desorption isotherm and the

dx.doi.org/10.1021/ic402468k | Inorg. Chem. 2014, 53, 998−1008

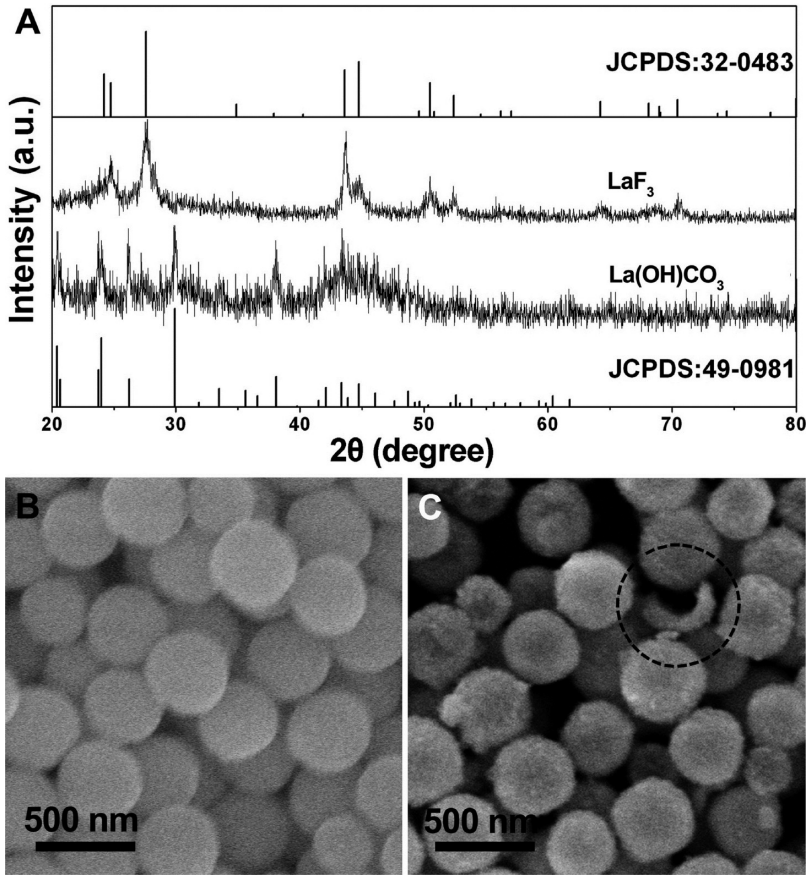

Figure 1. XRD patterns of the $La(OH)CO_3$ precursor and resulting LaF_3 sample (A) and SEM images of $La(OH)CO_3$ solid spheres (B) and LaF_3 hollow microspheres prepared for 3 h with an initial pH value of 3 (C).

Barrett–Joyner–Halenda method. UC emission spectra were acquired using a 980 nm LD module (K98D08M-30W, China) as the excitation source and detected by a R955 apparatus (Hamamatsu) from 400 to 750 nm. DC-PL was excited by a 150 W xenon lamp, and the excited spectra were recorded from 200 to 400 or 450 nm. The DOX concentration was detected by a UV-1601 UV–vis spectrophotometer, and the absorbance scan values were recorded with the specified 480 nm. The measurements above were wholly performed at room temperature.

RESULTS AND DISCUSSION

Phase, Structure, and Morphology of Hollow Spheres.

Phase, Structure, and Morphology of LaF_3 Hollow Spheres. It should be mentioned first that a low doping amount of Yb^{3+}/Er^{3+} (Ho^{3+} and Tm^{3+}), Ce^{3+}/Tb^{3+}, and Eu^{3+} does not change the phase or morphology of the final products. So. here LaF_3 and $LaCO_3F$ samples are taken as typical examples to elucidate the phase, shape, and structure of the doped products.

When the initial pH value of the second step is regulated to 3, the resulting product is LaF_3 hollow spheres, as shown in Figure 1. Figure 1A shows XRD patterns of the coprecipitated precursor and the resulting product. On the basis of the Joint Committee on Power Diffraction Standard (JCPDS) reference database, we can see clearly that the diffraction peaks of the precursor are well indexed to JCPDS no. 49-0981, which is orthorhombic $La(OH)CO_3$. Also, all of the diffraction peaks of the resulting product can coincide with the hexagonal phase LaF_3 (JCPDS no. 32-0483). Meanwhile, the diffraction peaks of the product are sharp and obvious, meaning that high crystallinity can be obtained at much lower reaction temperature (50 °C) and short time (3 h). That is because LaF_3 is easily precipitated because of the low solubility of fluoride itself, so LaF_3 hollow spheres would form quickly after mixing of $La(OH)CO_3$, H^+, and F^- ions. Parts B and C of Figure 1 indicate that there is an obvious similarity between the precursor and resulting product. $La(OH)CO_3$ and the resulting LaF_3 are both well-dispersed with an average diameter of 390 nm. Broken spheres in Figure 1C can prove that the spheres are hollow, with several shells corroded by H^+ ions in an acidic solution.

In order to ascertain the formation of hollow spheres, parts A–C of Figure 2 show TEM images with different magnifications of LaF_3 hollow spheres after reaction for 3 h. It is obvious that LaF_3 hollow microspheres with uniform morphology are obtained. Figure 2C indicates that the large hollow sphere consists of LaF_3 nanodisks. It is proposed that anions in the reacting solution, such as BF_4^-, NO_3^-, and BO_3^{3-}, are adsorbed on the (0001) plane of the crystal seed and suppress the crystal growth along the [0001] direction, and then 2D nanodisks are formed consequently.[40] HRTEM and FFT images (Figure 2D and inset) show that the interplanar distance between the adjacent lattice fringes is 0.32 nm, corresponding well to the *d*-spacing value of the $(11\bar{2}1)$ plane of the hexagonal phase LaF_3.

Phase, Structure, and Morphology of $LaCO_3F$ Hollow Spheres. If the initial pH value is unregulated and is about 6.2, the other phase $LaCO_3F$ is generated in place of LaF_3, as shown in Figure 3. From the XRD patterns, we can see that, after reaction for 40 min, the product is changed to a $La(OH)CO_3$

dx.doi.org/10.1021/ic402468k | Inorg. Chem. 2014, 53, 998–1008

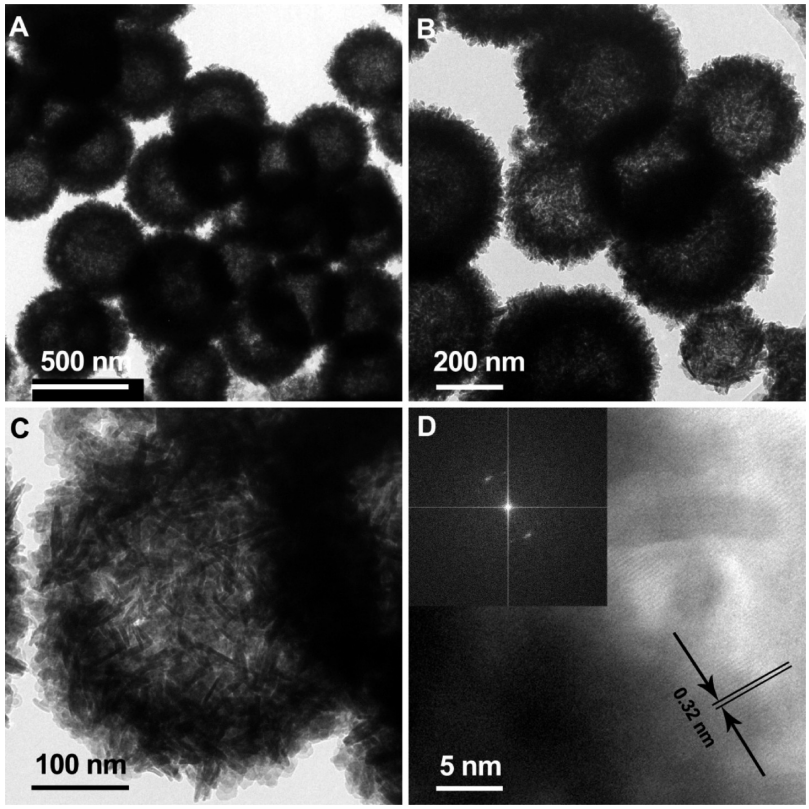

Figure 2. TEM images with different magnifications (A–C) and HRTEM image (D) of LaF_3 hollow microspheres. Inset in panel D: corresponding FFT image. The sample was prepared for 3 h with an initial pH value of 3.

and $LaCO_3F$ mixed phase. When the reaction time is 3 h, the diffraction peaks are thoroughly indexed to the hexagonal phase $LaCO_3F$ (JCPDS no. 41-0595). SEM images reveal that hollow spheres are evolved gradually and are consistent with XRD patterns. From Figure 3A, we can see that there are completely uniform solid $La(OH)CO_3$ spheres at the very beginning. With the reaction time increased to 40 min, uniform yolk-type $La(OH)CO_3$@$LaCO_3F$ spheres were obtained (Figure 3B). After reaction for 1 h (Figure 3C), still little $La(OH)CO_3$ survived in a few cores. In Figure 3D, uniform $LaCO_3F$ hollow spheres were obtained after reaction for 3 h. In the HRTEM image (Figure 3F), the interplanar distance between the adjacent lattice fringes of 0.35 nm matches well with the $(11\bar{2}0)$ plane of the hexagonal phase $LaCO_3F$. The FFT image (Figure 3F, inset) indicates that the resulting hollow spheres have many mesopores that make the lattice plane separate among the spheres.

The reason for generation of different products is due to the amount of H^+ ions in the initial solution. It is well-known that OH^- ions have the priority to react with H^+ ions. Only under conditions in which there are enough H^+ ions will CO_3^{2-} ions also be consumed by excess H^+ anions. When the initial pH value is not regulated with an average value of 6.2, the neutral environment is favorable to the existing of CO_3^{2-} ion, so $LaCO_3F$ hollow spheres are evolved in place of LaF_3.

Growth Mechanism of Hollow Spheres. As explained above, the morphology evolution of LaF_3 is similar to that of $LaCO_3F$, so the growth mechanism of $LaCO_3F$ is typically discussed. SEM images with lower magnification indicate that the resulting products are well-dispersed. TEM images of $LaCO_3F$ spheres are taken into account for the growth process in detail. Figure 4A shows that the $La(OH)CO_3$ precursor consists of well-dispersed solid spheres. From Figure 4B, yolk-type $La(OH)CO_3$@$LaCO_3F$ spheres are obtained after reaction for 40 min, which can be obviously proven by the solid inside and the resulting $LaCO_3F$ outside layers with the characteristic of *d*-spacing value of the $(11\bar{2}0)$ plane for the hexagonal phase $LaCO_3F$ (Figure 4B4). Parts C1–4 of Figure 4 are pure $LaCO_3F$ hollow spheres with nothing inside and an obvious shell. The formation of this hollow structure can be due to the Kirkendall effect, which is a new typical example to put this theory into a soft chemical method for getting hollow spheres.

There are two procedures during formation of the resulting products: The first procedure contains three collateral processes including dissolution of $La(OH)CO_3$, hydrolysis of $NaBF_4$, and reaction of H^+ ions with OH^- and CO_3^{2-}. $La(OH)CO_3$ can dissolve in La^{3+}, OH^-, and CO_3^{2-} under weak acidic conditions. $NaBF_4$ was slowly hydrolyzed to F^- and H^+ ions, which promote dissolution of $La(OH)CO_3$. The second procedure is the coprecipitation process to LaF_3 or $LaCO_3F$, which is decided by whether CO_3^{2-} is consumed in the first procedure. The whole reaction proceeds as follows:

$$La(OH)CO_3 \rightarrow La^{3+} + OH^- + CO_3^{2-} \quad (1\text{-}1)$$

$$BF_4^- + 3H_2O \rightarrow BO_3^{3-} + 6H^+ + 4F^- \quad (1\text{-}2)$$

$$3H^+ + OH^-(+CO_3^{2-}) \rightarrow H_2O(+CO_2) \quad (1\text{-}3)$$

$$La^{3+} + 3F^-(+CO_3^{2-}) \rightarrow LaF_3(LaCO_3F) \quad (2\text{-}1)$$

The formation of hollow spheres through a sacrificed-template method based on the Kirkendall effect is attributed to different diffusion rates between two components in a diffusion couple.[46] In this reaction process, the diffusion couples are La^{3+}

dx.doi.org/10.1021/ic402468k | *Inorg. Chem.* 2014, 53, 998–1008

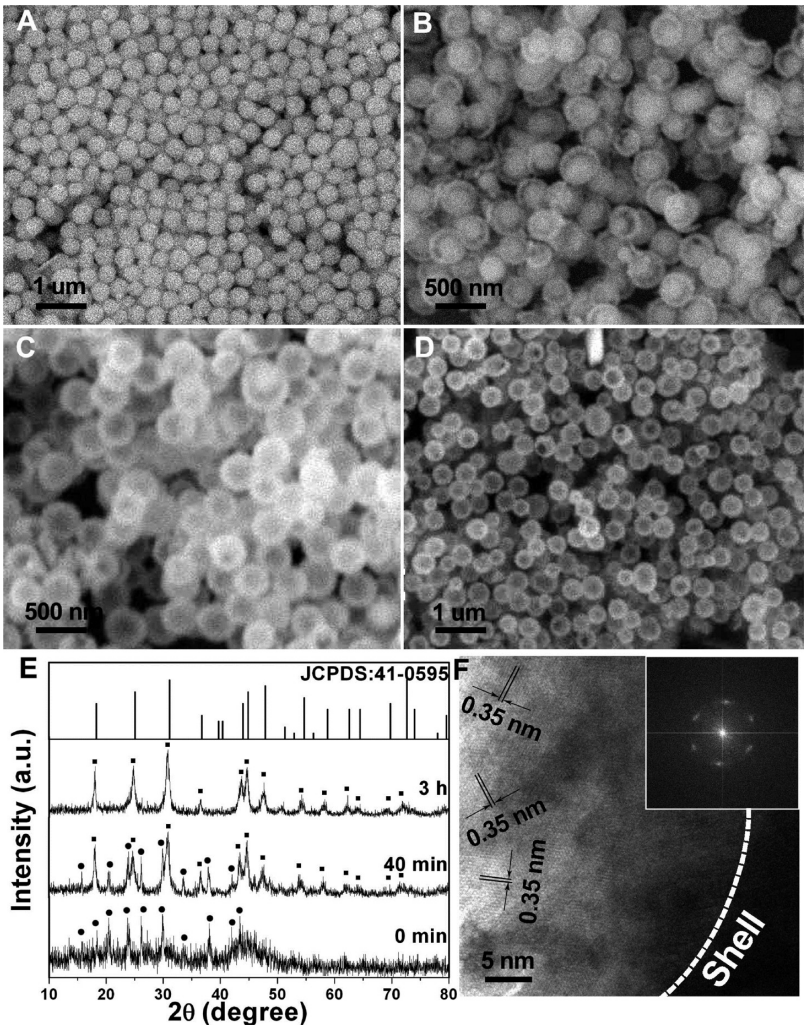

Figure 3. SEM images of the samples prepared with 0 h (A), 40 min (B), 1 h (C), and 3 h (D) with the initial pH value unregulated, XRD patterns of $LaCO_3F$ prepared with different reaction times (E), and HRTEM image of the $LaCO_3F$ sample prepared in 3 h (F). Inset in panel F: corresponding FFT image.

ions inside and F^- ions outside. The equilibrium constant of the hydrolysis reaction (1-2) is very small ($K = 6.41 \times 10^{-12}$),[42] which is helpful to keep the concentration of F^- ions in the reaction solution at a low level. The diffusion rate of F^- ions outside is slower than that of La^{3+} ions inside, and Kirkendall voids appear inside in order to make the diffusion balance.[30] With increasing time, the precursor inside is consumed and replaced by the increased pores, and the resulting product accumulates in the shell, and then hollow spheres consequently formed. The formation mechanism is simply presented in Scheme 1. The precursor was acquired in the typical process after 2 h. Through regulation of the initial pH value of the second step, different products of LaF_3 and $LaCO_3F$ hollow spheres were generated after 3 h. Also, we can see that a yolk-type $La(OH)CO_3$@$LaCO_3F$ sphere was formed after reaction for 40 min.

UC Luminescent Properties. The efficiency of energy conversion is mainly decided by the matching extent of the excitation photon energy and rare-earth-ion energy level, and the host material with low phonon energy also plays a significant role. Rare-earth fluorides have been extensively applied as UC-PL materials because of their low phonon energy, high luminous efficiency, and good stability.[47−53] In this section, the luminescent properties of LaF_3:Yb^{3+}/Er^{3+}, LaF_3:Yb^{3+}/Ho^{3+}, and LaF_3:Yb^{3+}/Tm^{3+} under 980 nm LD irradiation will be discussed.

UC Luminescence of LaF_3:Yb^{3+}/Er^{3+}. Figure 5A shows the UC emission spectrum of LaF_3:15% Yb^{3+}/1% Er^{3+}. The spectrum contains three chief emission peaks at around 521, 540, and 655 nm, corresponding to the respective $^2H_{11/2} \rightarrow {}^4I_{15/2}$, $^4S_{3/2} \rightarrow {}^4I_{15/2}$, and $^4F_{9/2} \rightarrow {}^4I_{15/2}$ transitions of Er^{3+}.[52−57] In addition, there is a weak emission peak assigned to $^2H_{9/2} \rightarrow {}^4I_{15/2}$ detected at 409 nm. Generally, this emission peak could not be observed easily because of the low efficiency of a three- or four-photon UC process and strong scattering of the host lattices. This appearance further proves that the resulting LaF_3 sample is a good host with high efficiency to emit strong light. The inset of Figure 5A represents a LaF_3:15% Yb^{3+}/1% Er^{3+} sample emitting strong green light under 980 nm LD irradiation.

It is well accepted that the output luminescent intensity (I) is a function of the infrared excitation power (P), which is signified by the formula $I \propto P^n$, where n is the number of photons absorbed by the ground-state level during the energy-transfer process. After the Napierian logarithm of blue, green, and red emissions and corresponding excitation powers are

dx.doi.org/10.1021/ic402468k | Inorg. Chem. 2014, 53, 998−1008

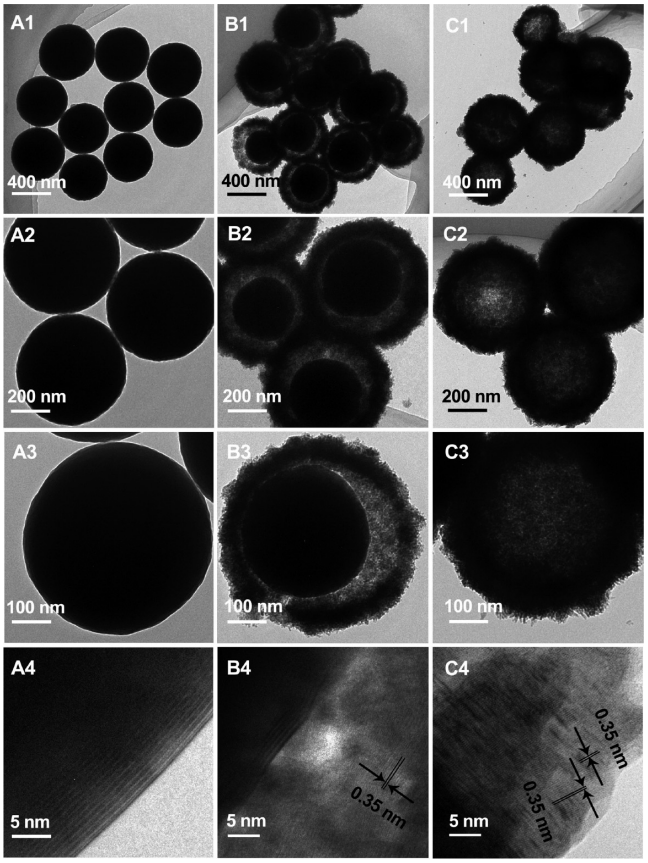

Figure 4. TEM images with different magnifications of the products prepared for 0 h (A), 40 min (B), and 3 h (C). All samples were prepared with the initial pH value unregulated.

taken, Figure 5B shows that the respective ratios are 2.405, 1.937, and 1.813, which indicates that the three emission processes are three-photon (blue light) and two-photon (green and red light) ones.

UC Luminescence of LaF_3:Yb^{3+}/Ho^{3+}. Figure 5C represents the UC emission spectrum of LaF_3:15% Yb^{3+}/1% Ho^{3+} under 980 nm LD excitation. There are two strong broad emission bands centered at 541−548 and 646−665 nm, which can be attributed to $^5F_4/^5S_2 \rightarrow {}^5I_8$ and $^5F_5 \rightarrow {}^5I_8$ transitions of Ho^{3+}, respectively.[58] The inset of Figure 5C reveals that the LaF_3:15% Yb^{3+}/1% Ho^{3+} sample emits strong pure green light. The power-dependent green and red emissions under 980 nm LD excitation are shown in Figure 5D. The slopes of the green and red emissions between the integral intensity and dependent power are 1.799 and 1.528, respectively. The result shows that the green- and red-emitting processes are both two-photon energy-transfer ones.

UC Luminescence of LaF_3:Yb^{3+}/Tm^{3+}. Figure 5E gives the emission spectrum of LaF_3:15% Yb^{3+}/1% Tm^{3+}. There are four peaks: intense blue emissions at 450 and 475 nm and weak red emission peaks at 645 and 698 nm, which are associated with $^1D_2 \rightarrow {}^3F_4$, $^1G_4 \rightarrow {}^3H_6$, $^1G_4 \rightarrow {}^3F_4$, and $^3F_3 \rightarrow {}^3H_6$ transitions of Tm^{3+}, respectively.[50,59,60] The inset represents LaF_3:15% Yb^{3+}/1% Tm^{3+} emitting strong purple light under 980 nm LD irradiation. Figure 5F shows that the respective ratios of blue and red emissions between the integral intensity and dependent power are 2.612 and 1.848, which indicates that they are three- and two-photon energy-transfer processes.

The corresponding CIE chromaticity coordinates of LaF_3:15% Yb^{3+}/1% Er^{3+}, LaF_3:15% Yb^{3+}/1% Ho^{3+}, and LaF_3:15% Yb^{3+}/1% Tm^{3+} emission spectra are calculated as (0.2194, 0.7356), (0.2500, 0.7256), and (0.1353, 0.0951), which correspond to points a−c in Figure S2A in the SI, respectively. Through the analysis above, the proposed UC mechanisms of LaF_3 doped with Yb^{3+}/Er^{3+}, Yb^{3+}/Ho^{3+}, and Yb^{3+}/Tm^{3+} are demonstrated in Figure S2B in the SI.

In order to evaluate the relative luminescent properties of the hollow structures with bulk structures, here we compared the two different morphologies of LaF_3. The bulk LaF_3 was precipitated by $La(NO_3)_3$ and NaF under a water solution with a temperature of 50 °C, and the morphology of bulk LaF_3 is shown in Figure S3 in the SI. Figure 6 shows that the emission spectra of the two samples are very similar with few differences because of their same f−f transitions, which are strongly shielded by the outside 5s and 5p electrons. LaF_3:15% Yb^{3+}/1% Er^{3+} in Figure 6A and LaF_3:15% Yb^{3+}/1% Ho^{3+} in Figure 6B show that there is slight decrease of their intensities, which is attributed to the surface defect of hollow structures. However, in our work, the luminescence intensity is enough for a drug carrier. In a further calculation, the intensity ratio of the energy transfer of $^4S_{3/2} \rightarrow {}^4I_{15/2}$ (540 nm) is 0.94:1 of LaF_3:15% Yb^{3+}/1% Er^{3+} between the hollow and bulk samples, and the intensity ratio of $^5F_4 \rightarrow {}^5I_8$ (541 nm) is 0.84:1. This result corresponds well with that in the reported literature.[60]

DC Luminescent Properties. Figure S4A in the SI shows excitation (monitored with an emission wavelength of 489 nm; left) and emission (excited at 272 nm; right) spectra of LaF_3:15% Ce^{3+}/5% Tb^{3+} (up) and $LaCO_3F$:15% Ce^{3+}/5% Tb^{3+} (down), respectively. Figure S4B in the SI is a CIE chromaticity photograph of LaF_3:15% Ce^{3+}/5% Tb^{3+} and $LaCO_3F$:15% Ce^{3+}/5% Tb^{3+}. The corresponding luminescent photographs are shown in Figure S4C in the SI. At the top of the picture are samples under daylight, and at the bottom of the picture are samples under UV irradiation. As shown in Figure S4A (left) in the SI, there is a big similarity between the two excitation

Scheme 1. Schematic Illustration for the Formation of LaF_3 and $LaCO_3F$ Hollow Microspheres

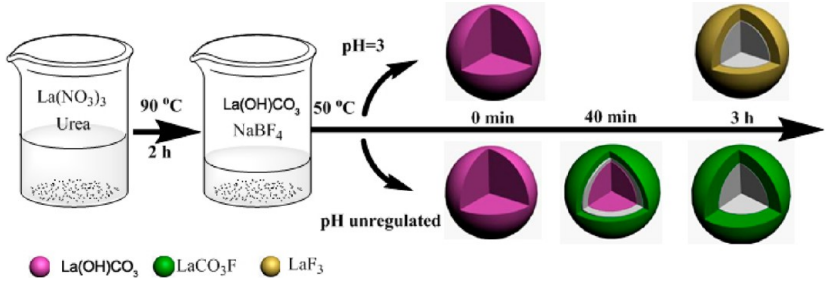

dx.doi.org/10.1021/ic402468k | Inorg. Chem. 2014, 53, 998−1008

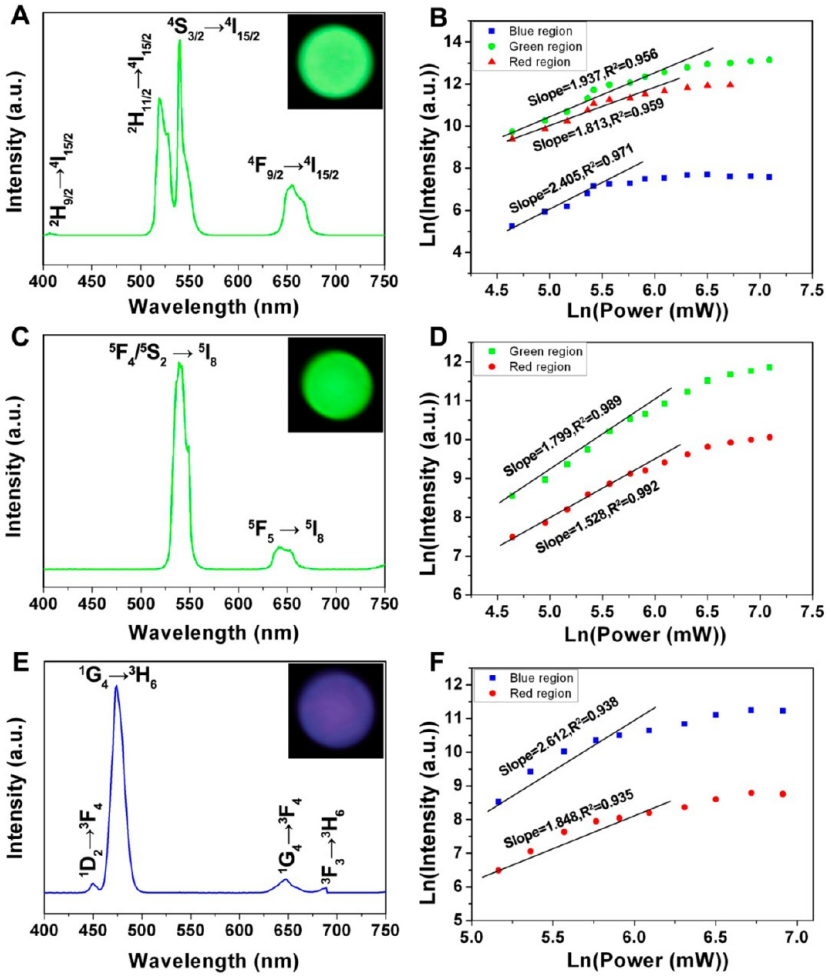

Figure 5. UC emission spectra and intensities as a function of the dependent pump power of LaF_3:15% Yb^{3+}/1% Er^{3+} (A and B), LaF_3:15% Yb^{3+}/1% Ho^{3+} (C and D), and LaF_3:15% Yb^{3+}/1% Tm^{3+} (E and F) under 980 nm LD excitation. Insets: their corresponding photographs under 980 nm LD irradiation.

spectra of LaF_3:Ce^{3+}/Tb^{3+} (up) and $LaCO_3F$:Ce^{3+}/Tb^{3+} (down). Both of them have a strong broad excitation peak near 240−300 nm and several weak broad excitation peaks between 300 and 380 nm (monitored with an emission wavelength of 489 nm). The strong broad excitation peak centered at around 272 nm is attributable to the absorption of 4f−5d transitions of Ce^{3+} ions, and the several weak peaks are due to f−f transitions of Tb^{3+}.[61,62] Figure S4A (right) in the SI displays the emission spectra of LaF_3:Ce^{3+}/Tb^{3+} and $LaCO_3F$:Ce^{3+}/Tb^{3+}. The emission spectra located from 450 to 650 nm are mainly composed of four strong peaks (489, 547, 584, and 621 nm), which separately correspond to the f−f transitions of Tb^{3+} from the excited $^5D_4$ levels to the ^7F_J (J = 6, 5, 4, 3) levels.[63,64]

In Figure S4B in the SI, it is clearly seen that the LaF_3:Ce^{3+}/Tb^{3+} sample has a yellow-green color and the $LaCO_3F$:Ce^{3+}/Tb^{3+} sample has a near-white color, respectively. Figure S4C in the SI shows that Ce^{3+}/Tb^{3+}-ion-doped LaF_3 and $LaCO_3F$ samples are white powders under daylight, while under UV irradiation, the as-synthesized LaF_3:Ce^{3+}/Tb^{3+} appear obviously bright yellow-green luminescent, and the light of $LaCO_3F$:Ce^{3+}/Tb^{3+} seemed weaker, which should be due to luminescence quenching caused by the higher vibrational energy (1439 cm^{-1}) of CO_3^{2-} in the $LaCO_3F$ host lattice,[26] which is also confirmed by the emission intensity difference of the two samples in Figure S4A in the SI.

Figure S5A in the SI shows excitation (monitored at 591 nm; left) and emission (excited at 396 nm; right) spectra of LaF_3:15% Eu^{3+} and $LaCO_3F$:15% Eu^{3+}, respectively. The corresponding photographs under daylight and under UV irradiation are given in Figure S5B in the SI. In Figure S5A (left) in the SI, the excitation spectra both have four narrow lines that are assigned to the characteristic f−f transitions of Eu^{3+}, including $^7F_0\rightarrow{}^5H_6$ (317 nm), $^7F_0\rightarrow{}^5D_4$ (374 nm), $^7F_0\rightarrow{}^5G_2$ (386 nm), and $^7F_0\rightarrow{}^5L_6$ (396 nm). Different from LaF_3:Eu^{3+}, there exists a broad band from 240 to 310 nm in the $LaCO_3F$:Eu^{3+} sample that is attributed to a charge-transfer band resulting from electron transfer from the ligand O^{2-} (2p) orbital to the empty states of the 4f configuration of Eu^{3+}.[65] There are mainly four emission lines in Figure S5A (right), which are due to the $^5D_0$ excited states to ^7F_J ground states of Eu^{3+}, i.e., 591 nm ($^5D_0\rightarrow{}^7F_1$), 617 nm ($^5D_0\rightarrow{}^7F_2$), 650 nm ($^5D_0\rightarrow{}^7F_3$), and 690 nm ($^5D_0\rightarrow{}^7F_4$).[66−71] It can also be seen that the emission intensity of LaF_3:Eu^{3+} is much higher than that of $LaCO_3F$:Eu^{3+}, which is also due to quenching by the higher vibrational energy (1439 cm^{-1}) of CO_3^{2-} in the $LaCO_3F$ host. Additionally, in the photographs of Figure S5B in the SI, pure red emissions can be achieved by 15% Eu^{3+}-doped LaF_3 and $LaCO_3F$ under UV irradiation. Also, we can easily see that

dx.doi.org/10.1021/ic402468k | Inorg. Chem. 2014, 53, 998−1008

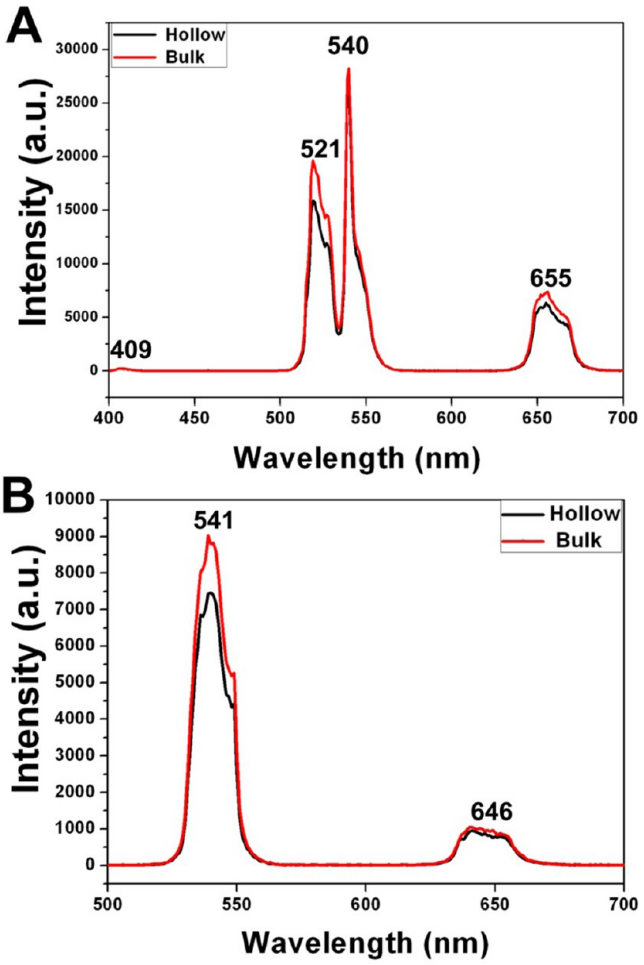

Figure 6. Emission spectra of LaF_3:15% Yb^{3+}/1% Er^{3+} (A) and LaF_3:15% Yb^{3+}/1% Ho^{3+} (B) with hollow particles (black line) and bulk phosphors (red line).

the LaF_3:Eu^{3+} sample exhibits stronger light than the $LaCO_3F$:Eu^{3+} sample.

Figure S6A in the SI shows emission spectra of LaF_3:*x*% Eu^{3+} with different doping concentrations (*x* = 5, 10, 15, 20, and 30), which is excited at 396 nm. We can see the emission regions kept at 591, 617, and 690 nm with only the intensity changed. The integral intensity of 591 and 617 nm as a function of the doping concentration is further calculated and exhibited in Figure S6B in the SI. With an increase of the Eu^{3+} doping concentration, the intensities of emission spectra increase gradually (5−15%), reach a maximum at 15%, then decrease a little, and remain almost stable afterward (20−30%). The decreased emission intensity is due to the concentration quenching effect at higher doping concentration. Generally, the doping concentration for luminescence quenching is 5% in LaF_3:Eu^{3+} bulk. However, the formation of nanospheres may suppress the cross-relaxation in order to increase the quenching concentration to 15%.[72]

Cell Viability, Drug Loading, and Release Properties. In order to better ascertain the formation of a mesoporous hollow structure, N_2 adsorption/desorption of the LaF_3:Yb/Er sample was measured, and the isotherm is given in Figure 7. It can be seen that the sample exhibits a typical IV-type isotherm with H1 hysteresis loops, which are characteristic of typical mesoporous materials.[43] The Brunauer−Emmett−Teller surface area and single pore volume (P/P_0 = 0.97) were calculated to be 54.9 m^2/g and 0.0913 cm^3/g, respectively. From Figure 7B, we can find the narrow size distribution (6.7 nm) of the sample. The mesoporous shell and hollow structure of the sample could provide the potential capability to be employed as a drug carrier for loading/carrying drug molecules.

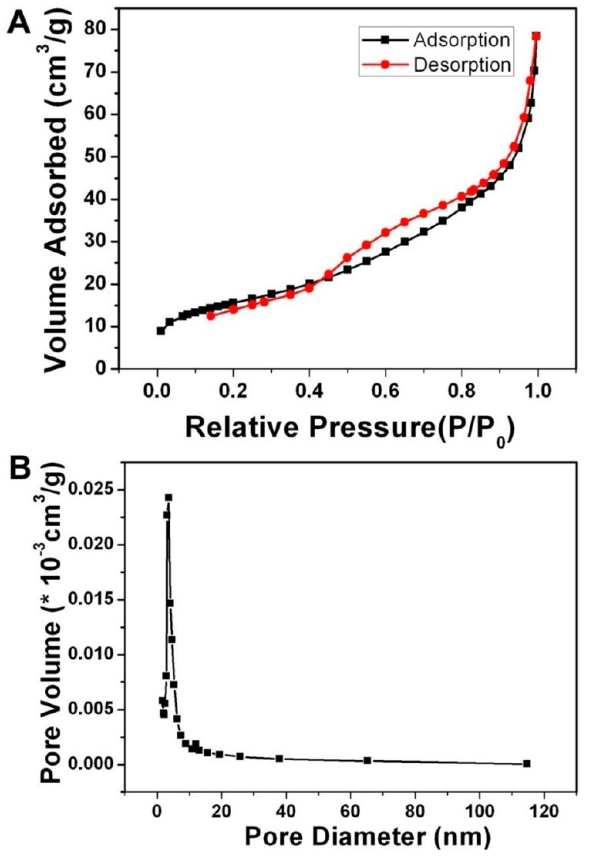

Figure 7. N_2 adsorption/desorption isotherm (A) and corresponding pore-size distribution curve (B) of LaF_3 hollow microspheres.

Cell Viability of LaF_3:Yb/Er and $LaCO_3F$:Ce/Tb. For potential biological application, the biocompatibility of the proposed material needs to be evaluated. A standard MTT cell assay was carried on L929 cell lines in order to detect the viability of LaF_3:Yb/Er and $LaCO_3F$:Ce/Tb hollow spheres. Figure 8 demonstrates the cell viability of LaF_3:Yb/Er and $LaCO_3F$:Ce/Tb samples incubated for 24 h with different concentrations varying from 7.8125 to 62.5 μg/mL. It is obvious that the viability of the as-prepared LaF_3:Yb/Er hollow spheres in all dosages is up to 95.3−110.9% and 103.5−109.3% to $LaCO_3F$:Ce/Tb hollow spheres. Even at a high-dosage concentration of 62.5 μg/mL, there are still 100.6% (LaF_3) and 109.3% ($LaCO_3F$) cells observed, respectively. The MTT assay data demonstrate that the two samples are nontoxic in a high amount to live cells. Therefore, LaF_3 and $LaCO_3F$ hollow spheres are both potentially applied in the biological field.

DOX Loading and Release of LaF_3:Yb/Er and $LaCO_3F$:Ce/Tb Samples. DOX was widely used as a model drug to evaluate the loading and release behaviors, and it was detected on the two samples. After stirred continuously and moderately for 24 h, DOX was almost convergent to LaF_3:Yb/Er and $LaCO_3F$:Ce/Tb with loading efficiencies of 84.3% and 78.4%, respectively. The results are much higher than those of the solid mesoporous material, which is only 23.6−48.2% loaded.[73]

dx.doi.org/10.1021/ic402468k | *Inorg. Chem.* 2014, 53, 998−1008

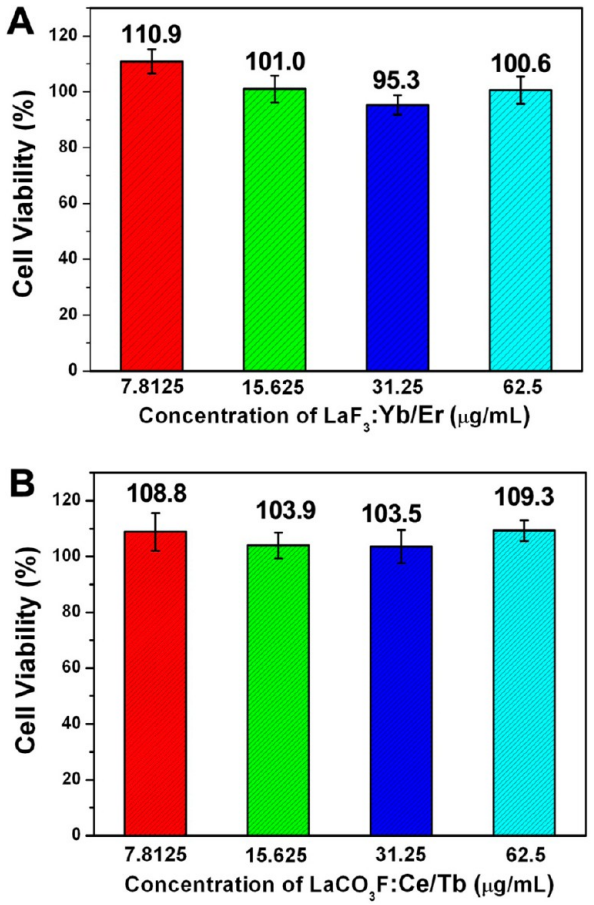

Figure 8. L929 fibroblast cell viability of LaF_3:Yb/Er (A) and $LaCO_3F$:Ce/Tb (B) hollow spheres incubated for 24 h.

Meanwhile, pH-dependent drug release behavior has been detected in different released environments. Here, pH values of 4 and 7 were selected to study the release properties, which represent the environments of cancer and normal cells, respectively. As shown in Figure 9, when the pH value is 7, there is little difference between LaF_3:Yb/Er and $LaCO_3F$:Ce/Tb with release efficiencies of 35.8% and 36.4%. Compared with the pH value of 7, the two carriers show much faster release efficiencies when the pH value is 4, and $LaCO_3F$:Ce/Tb reaches up to 90.0%, which is much higher than LaF_3:Yb/Er with a release efficiency of 59.8%. For $LaCO_3F$:Ce/Tb, during the initial stage, 68.3% of DOX was released, which is much bigger than 41.3% of LaF_3:Yb/Er. There are two factors attributing to the release efficiencies between $LaCO_3F$ and LaF_3 in different pH value conditions. One factor is the different mesoporous structures of the two samples. Close observation of the TEM images (Figures 2 and 4C) reveals that the microstructures of the two samples are very different. The size of the nanoparticles comprising the $LaCO_3F$ hollow spheres is much smaller than those of the LaF_3 hollow spheres, and the distribution of the $LaCO_3F$ hollow spheres is relatively higher. The other factor is the different release efficiencies under different pH conditions. Therefore, when the pH value is 7, the release efficiencies of the two samples are both slow because of the strong interaction between the surface and DOX molecules, and the different structures do not work, resulting in little difference in the release efficiencies between the two samples. It is well accepted that the low pH value is beneficial to DOX release. When the pH value is 4, the released fraction is much larger than that obtained with a pH value of 7, which should be related with the difference of their microstructures.

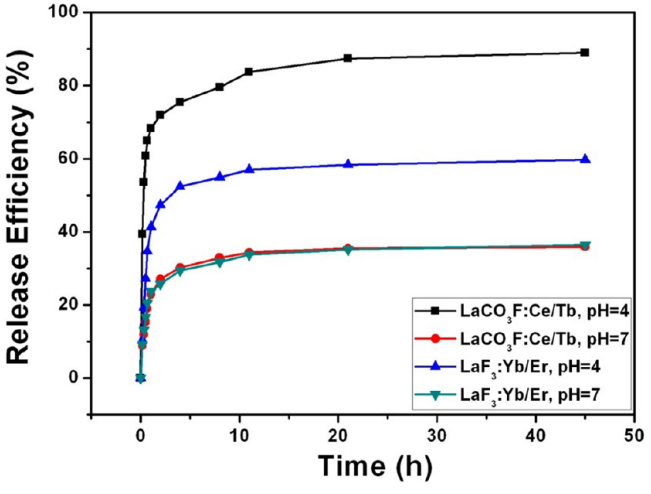

Figure 9. DOX release efficiencies of DOX-LaF_3:Yb/Er and DOX-$LaCO_3F$:Ce/Tb hollow microspheres with release times at pH values of 4 and 7.

The observed release properties (rapid release followed by a plateau) can be explained by simple adsorption of the drug to the surface of the hollow spheres. DOX adsorbed weakly on the outer surfaces or near the pore entrances is rapidly leached in the initial process, while the drug adsorbed in the inner surfaces or channels of the pores by strong interaction between drug molecules and the hydrogen bonds on the inner surface will release in a sustained procedure. This is well consistent with other literature that had been tested in a similar experiment.[74] It should be noted that the initially rapid release of DOX molecules is essential to curing cancer, and the slow release of the rest of the drug molecules can be continued for curbing the few surviving cells. In conclusion, there is no doubt that the release property of LaF_3:Yb/Er is outstanding; however, $LaCO_3F$:Ce/Tb provides a wide choice for biological application as a drug carrier and targeted drug delivery. In particular, fluorescence of the functional material allows it to be tracked or monitored during the release process.

CONCLUSIONS

In summary, we proposed a facile, mild, and mass-production method to synthesize hollow mesoporous LaF_3 and $LaCO_3F$ spheres. $La(OH)CO_3$ was prepared as the sacrificed template, and $NaBF_4$ was chosen as the fluorine source. The as-prepared spheres are formed from solid to yolk-type spheres and generated hollow spheres after 3 h with a low temperature of 50 °C. Similar to the UC luminescent properties of LaF_3 doped with Yb^{3+}/Er^{3+}, Yb^{3+}/Ho^{+} emits strong green light and LaF_3:Yb^{3+}/Tm^{3+} strong purple light under 980 nm LD irradiation. The DC luminescent properties of Ce^{3+}/Tb^{3+}-doped LaF_3 and $LaCO_3F$ emit bright yellow-green and near-white light under UV irradiation, respectively. LaF_3:Eu^{3+} and $LaCO_3F$:Eu^{3+} are both red light under UV irradiation. By varying the concentration of Eu^{3+}, we can see a quenching concentration is up to 15% due to the microstructure. Moreover, as potential biomaterials, the hollow microspheres were employed as drug carriers to study the DOX sustained and release performances. We can conclude that the as-

dx.doi.org/10.1021/ic402468k | Inorg. Chem. 2014, 53, 998−1008

prepared multifunctional material could potentially be used in the drug release field.

■ ASSOCIATED CONTENT

Supporting Information

Absorbance spectrum, absorbance versus concentration plot, CIE chromaticity diagrams, proposed energy-transfer mechanism, bulk LaF_3, DC excitation and emission spectra, luminescent photographs, and integral intensity versus doping concentration plot. This material is available free of charge via the Internet at http://pubs.acs.org.

■ AUTHOR INFORMATION

Corresponding Authors

*E-mail: gaishili@hrbeu.edu.cn.
*E-mail: yangpiaoping@hrbeu.edu.cn.

Notes

The authors declare no competing financial interest.

■ ACKNOWLEDGMENTS

Financial support from the National Natural Science Foundation of China (Grant NSFC 21271053), Research Fund for the Doctoral Program of Higher Education of China (Grant 20112304110021), Natural Science Foundation of Heilongjiang Province (Grant LC2012C10), Program for New Century Excellent Talents in University, Harbin Sci.-Tech. Innovation Foundation (Grant RC2012XK017012), and the Fundamental Research Funds for the Central Universities of China is gratefully acknowledged.

■ REFERENCES

(1) Xu, Z. P.; Zeng, Q. H.; Lu, G. Q.; Yu, A. B. *Chem. Eng. Sci.* **2006**, *61*, 1027.
(2) Lanza, G. M.; Yu, X.; Winter, P. M.; Abendschein, D. R.; Karukstis, K. K.; Scott, M. J.; Chinen, L. K.; Fuhrhop, R. W.; Scherrer, D. E.; Wickline, S. A. *Circulation* **2002**, *106*, 2842.
(3) Tan, Y. W.; Bai, F.; Wang, D. S.; Peng, Q.; Wang, X.; Li, Y. D. *Chem. Mater.* **2007**, *19*, 5773.
(4) Jiao, Y. F.; Guo, J.; Shen, S.; Chang, B. S.; Zhang, Y. H.; Jiang, X. G.; Yang, W. L. *J. Mater. Chem.* **2012**, *22*, 17636.
(5) Wang, G.; Peng, Q.; Li, Y. *Acc. Chem. Res.* **2011**, *44*, 322.
(6) Wang, T.; Zhang, L.; Su, Z.; Wang, C.; Liao, Y.; Fu, Q. *ACS Appl. Mater. Interfaces* **2011**, *3*, 2479.
(7) Li, L.; Ding, J.; Xue, J. M. *Chem. Mater.* **2009**, *21*, 3629.
(8) De Cock, L. J.; De Koker, S.; De Geest, B. G.; Grooten, J.; Vervaet, C.; Remon, J. P.; Sukhorukov, G. B.; Antipina, M. N. *Angew. Chem., Int. Ed.* **2010**, *49*, 6954.
(9) Zhao, W. R.; Chen, H. R.; Li, Y. S.; Li, L.; Lang, M. D.; Shi, J. L. *Adv. Funct. Mater.* **2008**, *18*, 2780.
(10) Feng, Z.; Li, Y.; Niu, D.; Li, L.; Zhao, W.; Chen, H.; Li, L.; Gao, J.; Ruan, M.; Shi, J. *Chem. Commun.* **2008**, 2629.
(11) Yang, G. X.; Gai, S. L.; Qu, F. Y.; Yang, P. P. *ACS Appl. Mater. Interfaces* **2013**, *5*, 5788.
(12) Wang, Z. L.; Hao, J. H.; Chan, H. L. W. *J. Mater. Chem.* **2010**, *20*, 3178.
(13) Liu, Y. S.; Tu, D. D.; Zhu, H. M.; Chen, X. Y. *Chem. Soc. Rev.* **2013**, *42*, 6924.
(14) Wang, F.; Deng, R. R.; Wang, J.; Wang, W. X.; Han, Y.; Zhu, M.; Chen, X. Y.; Liu, X. G. *Nat. Mater.* **2011**, *10*, 968.
(15) Haase, M.; Schafer, H. *Angew. Chem., Int. Ed.* **2011**, *50*, 5808.
(16) Abel, K. A.; Boyer, J. C.; van Veggel, F. C. J. M. *J. Am. Chem. Soc.* **2009**, *131*, 14644.
(17) Li, Z. Q.; Zhang, Y.; Jiang, S. *Adv. Mater.* **2008**, *20*, 4765.
(18) Yi, G. S.; Lu, H. C.; Zhao, S. Y.; Yue, G.; Yang, W. J.; Chen, D. P.; Guo, L. H. *Nano Lett.* **2004**, *4*, 2191.
(19) Boyer, J. C.; Cuccia, L. A.; Capobianco, J. A. *Nano Lett.* **2007**, *7*, 847.
(20) Kumar, R.; Nyk, M.; Ohulchanskyy, T. Y.; Flask, C. A.; Prasad, P. N. *Adv. Funct. Mater.* **2009**, *19*, 853.
(21) Ptacek, P.; Schafer, H.; Kompe, K.; Haase, M. *Adv. Funct. Mater.* **2007**, *17*, 3843.
(22) Ju, Q.; Tu, D. T.; Liu, Y. S.; Li, R. F.; Zhu, H. M.; Chen, J. C.; Chen, Z.; Huang, M. D.; Chen, X. Y. *J. Am. Chem. Soc.* **2012**, *134*, 1323.
(23) Sivakumar, S.; Diamente, P. R.; van Veggel, F. C. J. M. *Chem.—Eur. J.* **2006**, *12*, 5878.
(24) Wang, Z. L.; Quan, Z. W.; Jia, P. Y.; Lin, C. K.; Luo, Y.; Chen, Y.; Fang, J.; Zhou, W.; O'Connor, C. J.; Lin, J. *Chem. Mater.* **2006**, *18*, 2030.
(25) Wang, L. Y.; Li, P.; Li, Y. D. *Adv. Mater.* **2007**, *19*, 3304.
(26) Shang, M.; Li, G.; Kang, X.; Yang, D.; Geng, D.; Peng, C.; Cheng, Z.; Lian, H.; Lin, J. *Dalton Trans.* **2012**, *41*, 5571.
(27) Stouwdam, J. W.; van Veggel, F. *Langmuir* **2004**, *20*, 11763.
(28) Wang, X.; Zhuang, J.; Peng, Q.; Li, Y. *Inorg. Chem.* **2006**, *45*, 6661.
(29) Mai, H. X.; Zhang, Y. W.; Si, R.; Yan, Z. G.; Sun, L. D.; You, L. P.; Yan, C. H. *J. Am. Chem. Soc.* **2006**, *128*, 6426.
(30) Li, C.; Lin, J. *J. Mater. Chem.* **2010**, *20*, 6831.
(31) Zhuang, J. L.; Yang, X. F.; Fu, J. X.; Liang, C. L.; Wu, M. M.; Wang, J.; Su, Q. *Cryst. Growth Des.* **2013**, *13*, 2292.
(32) Yang, P. P.; Gai, S. L.; Lin, J. *Chem. Soc. Rev.* **2012**, *41*, 3679.
(33) Liu, J.; Qiao, S. Z.; Hartono, S. B.; Lu, G. Q. *Angew. Chem., Int. Ed.* **2010**, *49*, 4981.
(34) Tian, G.; Gu, Z. J.; Liu, X. X.; Zhou, L. J.; Yin, W. Y.; Yan, L.; Jin, S.; Ren, W. L.; Xing, G. M.; Li, S. J.; Zhao, Y. L. *J. Phys. Chem. C* **2011**, *115*, 23790.
(35) Jia, G.; You, H. P.; Liu, K.; Zheng, Y. H.; Guo, N.; Zhang, H. J. *Langmuir* **2010**, *26*, 5122.
(36) Dong, W. F.; Ferri, J. K.; Adalsteinsson, T.; Schonhoff, M.; Sukhorukov, G. B.; Mohwald, H. *Chem. Mater.* **2005**, *17*, 2603.
(37) Khanal, A.; Inoue, Y.; Yada, M.; Nakashima, K. *J. Am. Chem. Soc.* **2007**, *129*, 1534.
(38) Cheng, X. J.; Chen, M.; Wu, L. M.; Gu, G. X. *Langmuir* **2006**, *22*, 3858.
(39) Li, J.; Zeng, H. C. *J. Am. Chem. Soc.* **2007**, *129*, 15839.
(40) Fan, H. J.; Knez, M.; Scholz, R.; Hesse, D.; Nielsch, K.; Zacharias, M.; Gosele, U. *Nano Lett.* **2007**, *7*, 993.
(41) Zhang, F.; Shi, Y. F.; Sun, X. H.; Zhang, D.; Stucky, G. D. *Chem. Mater.* **2009**, *21*, 5237.
(42) Zhao, J. W.; Liu, X. M.; Cui, D.; Sun, Y. J.; Yu, Y.; Yang, Y. F.; Du, C.; Wang, Y.; Song, K.; Liu, K.; Lu, S. Z.; Kong, X. G.; Zhang, H. *Eur. J. Inorg. Chem.* **2010**, 1813.
(43) Dai, Y. L.; Zhang, C. M.; Cheng, Z. Y.; Ma, P. A.; Li, C. X.; Kang, X. J.; Yang, D. M.; Lin, J. *Biomaterials* **2012**, *33*, 2583.
(44) Hou, Z. Y.; Li, C. X.; Ma, P. A.; Cheng, Z. Y.; Li, X. J.; Zhang, X.; Dai, Y. L.; Yang, D. M.; Liang, H. Z.; Lin, J. *Adv. Funct. Mater.* **2012**, *22*, 2713.
(45) Zhu, L.; Meng, I.; Cao, X. Q. *Eur. J. Inorg. Chem.* **2007**, 3863.
(46) Yin, Y. D.; Rioux, R. M.; Erdonmez, C. K.; Hughes, S.; Somorjai, G. A.; Alivisatos, A. P. *Science* **2004**, *304*, 711.
(47) Jia, L. P.; Zhang, Q.; Yan, B. *Mater. Res. Bull.* **2012**, *47*, 3301.
(48) Liang, X.; Wang, X.; Zhuang, J.; Peng, Q.; Li, Y. D. *Adv. Funct. Mater.* **2007**, *17*, 2757.
(49) Wang, Z. Y.; Wang, L. M.; Li, Z. Q. *Mater. Lett.* **2011**, *65*, 3516.
(50) Yin, A. X.; Zhang, Y. W.; Sun, L. D.; Yan, C. H. *Nanoscale* **2010**, *2*, 953.
(51) Zhang, C. M.; Ma, P. A.; Li, C. X.; Li, G. G.; Huang, S. S.; Yang, D. M.; Shang, M. M.; Kang, X. J.; Lin, J. *J. Mater. Chem.* **2011**, *21*, 717.
(52) Zhang, Q.; Yan, B. *Inorg. Chem.* **2010**, *49*, 6834.
(53) Zhang, Q.; Yan, B. *Chem. Commun.* **2011**, *47*, 5867.
(54) Feng, W.; Sun, L. D.; Yan, C. H. *Chem. Commun.* **2009**, 4393.
(55) Zhang, F.; Braun, G. B.; Shi, Y.; Zhang, Y.; Sun, X.; Reich, N. O.; Zhao, D.; Stucky, G. *J. Am. Chem. Soc.* **2010**, *132*, 2850.

(56) Zhang, F.; Wan, Y.; Yu, T.; Zhang, F.; Shi, Y.; Xie, S.; Li, Y.; Xu, L.; Tu, B.; Zhao, D. *Angew. Chem., Int. Ed.* **2007**, *46*, 7976.
(57) Hao, J. H.; Zhang, Y.; Wei, X. H. *Angew. Chem., Int. Ed.* **2011**, *50*, 6876.
(58) Shan, J.; Qin, X.; Yao, N.; Ju, Y. *Nanotechnology* **2007**, *18*, 445607.
(59) Liu, N.; Qin, W. P.; Qin, G. S.; Jiang, T.; Zhao, D. *Chem. Commun.* **2011**, *47*, 7671.
(60) He, F.; Yang, P.; Wang, D.; Li, C.; Niu, N.; Gai, S.; Zhang, M. *Langmuir* **2011**, *27*, 5616.
(61) Ghosh, P.; Kar, A.; Patra, A. *Nanoscale* **2010**, *2*, 1196.
(62) Wang, L. Y.; Li, Y. D. *Chem.—Eur. J.* **2007**, *13*, 4203.
(63) Ju, Q. A.; Luo, W. Q.; Liu, Y. S.; Zhu, H. M.; Li, R. F.; Chen, X. Y. *Nanoscale* **2010**, *2*, 1208.
(64) Liu, W.-R.; Lin, C. C.; Chiu, Y.-C.; Yeh, Y.-T.; Jang, S.-M.; Liu, R.-S.; Cheng, B.-M. *Opt. Express* **2009**, *17*, 18103.
(65) Yaiphaba, N.; Ningthoujam, R. S.; Singh, N. S.; Vatsa, R. K.; Singh, N. R. *J. Lumin.* **2010**, *130*, 174.
(66) Sun, X.; Zhang, Y.-W.; Du, Y.-P.; Yan, Z.-G.; Si, R.; You, L.-P.; Yan, C.-H. *Chem.—Eur. J.* **2007**, *13*, 2320.
(67) Zheng, Y.; You, H.; Jia, G.; Liu, K.; Song, Y.; Yang, M.; Zhang, H. *Cryst. Growth Des.* **2009**, *9*, 5101.
(68) Chen, L.; Chen, K.-J.; Lin, C.-C.; Chu, C.-I.; Hu, S.-F.; Lee, M.-H.; Liu, R.-S. *J. Comb. Chem.* **2010**, *12*, 587.
(69) Liu, Y.; Tu, D.; Zhu, H.; Li, R.; Luo, W.; Chen, X. *Adv. Mater.* **2010**, *22*, 3266.
(70) Zhang, L.; Jia, G.; You, H.; Liu, K.; Yang, M.; Song, Y.; Zheng, Y.; Huang, Y.; Guo, N.; Zhang, H. *Inorg. Chem.* **2010**, *49*, 3305.
(71) Liu, W.-R.; Lin, C. C.; Chiu, Y.-C.; Yeh, Y.-T.; Jang, S.-M.; Liu, R.-S. *Opt. Express* **2010**, *18*, 2946.
(72) Meng, J.-X.; Zhang, M.-F.; Liu, Y.-L.; Man, S.-Q. *Spectrochim. Acta, Part A* **2007**, *66*, 81.
(73) Zhao, Q.; Wang, T.; Wang, J.; Zheng, L.; Jiang, T.; Cheng, G.; Wang, S. *J. Non-Cryst. Solids* **2012**, *358*, 229.
(74) Zhang, C.; Li, C.; Peng, C.; Chai, R.; Huang, S.; Yang, D.; Cheng, Z.; Lin, J. *Chem.—Eur. J.* **2010**, *16*, 5672.